RESEARCH ARTICLE
PLANETARY SCIENCE

Earth and Planetary Physics
2: 1–14, 2018
doi: 10.26464/epp2018001

Radiation belt electron scattering by whistler-mode chorus in the Jovian magnetosphere: Importance of ambient and wave parameters

BinBin Ni[1,2*], Jing Huang[1], YaSong Ge[3], Jun Cui[4], Yong Wei[3], XuDong Gu[1], Song Fu[1], Zheng Xiang[1], and ZhengYu Zhao[1]

[1]Department of Space Physics, School of Electronic Information, Wuhan University, Wuhan 430072, China;

[2]Lunar and Planetary Science Laboratory, Macau University of Science and Technology-Partner Laboratory of Key Laboratory of Lunar and Deep Space Exploration, Chinese Academy of Sciences, Macau;

[3]Key Laboratory of Earth and Planetary Physics, Institute of Geology and Geophysics, Chinese Academy of Sciences, Beijing 100029, China;

[4]School of Atmospheric Sciences, Sun Yat-Sen University, Zhuhai Guangdong 519082, China

Abstract: Whistler-mode chorus waves are regarded as an important acceleration mechanism contributing to the formation of relativistic and ultra-relativistic electrons in the Jovian radiation belts. Quantitative determination of the chorus wave driven electron scattering effect in the Jovian magnetosphere requires detailed information of both ambient magnetic field and plasma density and wave spectral property, which however cannot be always readily acquired from observations of existed missions to Jupiter. We therefore perform a comprehensive analysis of the sensitivity of chorus induced electron scattering rates to ambient magnetospheric and wave parameters in the Jovian radiation belts to elaborate to which extent the diffusion coefficients depend on a number of key input parameters. It is found that quasi-linear electron scattering rates by chorus can be strongly affected by the ambient magnetic field intensity, the wave latitudinal coverage, and the peak frequency and bandwidth of the wave spectral distribution in the Jovian magnetosphere, while they only rely slightly on the background plasma density profile and the peak wave normal angle, especially when the wave emissions are confined at lower latitudes. Given the chorus wave amplitude, chorus induced electron scattering rates strongly depend on Jovian *L*-shell to exhibit a tendency approximately proportional to L_J^3. Our comprehensive analysis explicitly demonstrates the importance of reliable information of both the ambient magnetospheric state and wave distribution property to understanding the dynamic electron evolution in the Jovian radiation belts and therefore has implications for future mission planning to explore the extreme particle radiation environment of Jupiter and its satellites.

Keywords: Jovian radiation belts; whistler-mode chorus; resonant wave-particle interactions; magnetospheric state

Citation: Ni, B. B., Huang, J., Ge, Y. S., Cui, J., Wei, Y., Gu, X. D., Fu, S., Xiang, Z., and Zhao, Z. Y. (2018). Radiation belt electron scattering by whistler-mode chorus in the Jovian magnetosphere: Importance of ambient and wave parameters. *Earth Planet. Phys.*, *2*, 1–14. http://doi.org/10.26464/epp2018001

1. Introduction

In the solar system, the radiation belts of Jupiter are most intense among all the planets (Bolton et al., 2002). The first observations of decimetric wavelength emissions (10 s to 100 s of cm) (e.g., Burke and Franklin, 1955; Drake and Hvatum, 1959; Radhakrishnan and Roberts, 1960) provided evidence of the presence of trapped radiation in the Jovian magnetosphere (e.g., Carr and Gulkis, 1969; Berge and Gulkis, 1976; Bolton et al., 2002). While radial diffusion, interactions with neutrals, and synchrotron radiation loss have been intensively investigated as mechanisms accounting for the acceleration of Jovian radiation belt relativistic electrons (Gerard, 1970, 1976; Klein, 1976; Klein et al., 1989; Santos-Costa and Bourdarie, 2001; Santos-Costa et al., 2008), wave-particle interactions, while fundamental and important, receive relatively less attention. As one piece of pioneer work, Horne et al. (2008) developed a basic model of whistler mode waves at Jupiter to demonstrate that intense whistler-mode waves are strong enough to accelerate Jovian radiation belt electrons to relativistic energies. A later study of Shprits et al. (2012) performed a comparative study to investigate the effect of chorus wave induced pitch angle and energy diffusion at Earth, Jupiter, and Saturn, confirming that interactions with whistler waves are responsible for significant local acceleration of electrons at Jupiter, and suggesting that the wave latitudinal distribution has a determining role in the dynamics of energetic electrons. Most recently, De Soria-Santacruz et al. (2016) presented an empirical model of the energetic electron environment in Jupiter's magnetosphere, which is named as the Galileo Interim Radiation Electron Model version-2 (GIRE2).

Apparently, as an important acceleration mechanism of relativist-

Correspondence to: B. B. Ni, bbni@whu.edu.cn
Received 29 JUL 2017; Accepted 16 SEP 2017.
Accepted article online 10 OCT 2017.

ic and ultra-relativistic electrons in the Jovian radiation belts (Woodfield et al., 2013, 2014), chorus wave driven scattering coefficients not only provide straightforward information of the wave impact on electrons but also act as essential inputs for diffusion simulations of electron dynamic evolution. Their quantitative determination requires detailed information of both ambient magnetic field and plasma density and wave spectral property, which however cannot be always readily acquired from spacecraft observations. While previous studies explored the sensitivity of chorus wave induced electron scattering rates to the wave latitudinal coverage, wave normal angle, plasma density model and so on in the Jovian magnetosphere (e.g., Horne et al., 2008; Shprits et al., 2012; De Soria-Santacruz et al., 2016), a further detailed analysis is necessary to figure out how the diffusion coefficients depend on a full group of important ambient magnetospheric and wave parameters, which is the focus of the present study.

The paper is organized as follows. Section 2 describes the basic models of ambient magnetic field, plasma density and wave spectral intensity adopted in the context of Jupiter's magnetosphere for this comprehensive analysis. In section 3, we investigate in detail the variations of Jovian radiation belt electron scattering rates by chorus waves with ambient magnetic field strength, plasma density profile, wave latitudinal coverage, peak wave frequency, wave spectral bandwidth, and Jovian L-shell. Normalized differences or ratios between the model results corresponding to different parameter selections are evaluated to quantitatively specify the diverse importance of ambient and wave parameters, which is followed by discussions and conclusions in section 4.

2. Model Description

In the present study, we focus on the spatial region of typically intense radiation environment in the Jovian magnetosphere, say, the Jovian L-shells of L_J = 6–10. The ambient magnetic field profile can be reasonably approximated as a dipole model (Khurana et al., 1997), given by

$$B = B_{eq}\left(1+3\sin^2\lambda\right)^{1/2}/\cos^6\lambda, \tag{1}$$

where $B_{eq}=B_0/L_J^3$ is the equatorial magnetic field and λ is the magnetic latitude. Regarding the background plasma density, we follow previous studies (Shprits et al., 2012) to select three different electron density models for sensitivity analysis:

Density Model 1 (DM1) :

$$N(L_J,\lambda) = N_{eq}(L_J), \tag{2}$$

Density Model 2 (DM2) :

$$N(L_J,\lambda) = N_{eq}(L_J)\left[\left(1+3\sin^2\lambda\right)^{1/2}/\cos^6\lambda\right]^{-1}, \tag{3}$$

Density Model 3 (DM3) :

$$N(L_J,\lambda) = N_{eq}(L_J)\exp\left[-L_J^2\left(1-\cos^6\lambda\right)/\left(3H^2\right)\right], \tag{4}$$

where

$$N_{eq} = 3.2\times10^8 L_J^{-6.9}\,\mathrm{cm}^{-3} \tag{5}$$

is the equatorial plasma density as a function of the Jovian L-shell (L_J) following the study of Bagenal and Delamere (2011), $H = 10^{a_1+a_2r+a_3r^2+a_4r^3+a_5r^4}$ is the scale height with r=log$_{10}$ (L_J) and a set of parameters a_1 = –0.116, a_2 =2.14, a_3 = –2.05, a_4 = 0.491, and a_5 = 0.126. Note that DM3 is adopted following the study of Persoon et al. (2006). Figure 1 displays the plasma density variations with magnetic latitude for the above three models at L_J = 8. Apparently, DM1 is latitudinally constant, while DM2 and DM3 are latitudinally variable. The change of DM2 is more pronounced compared to DM3. The differences between different models are more apparent as the latitude increases. It is worthwhile to note that the differences are quite small for $|\lambda|$<15°.

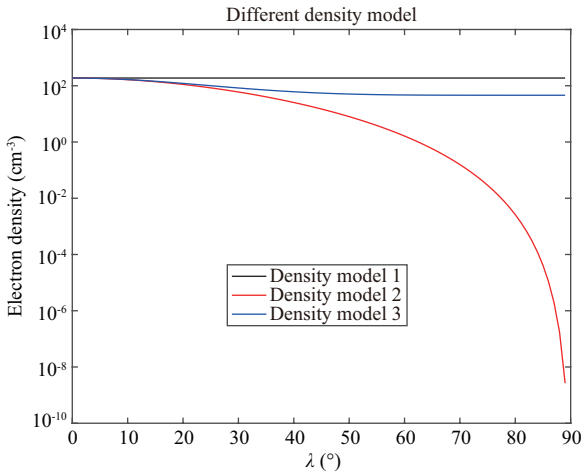

Figure 1. Plasma density variations with magnetic latitude for the considered three models (described by equations (1)–(3)) at L_J = 8.

Concerning the chorus wave distribution model in the Jovian magnetosphere, we follow previous studies (Glauert and Horne, 2005) to assume that both the wave frequency spectrum and wave normal angle distribution are Gaussian. Specifically, the wave power spectral density $B^2(\omega)$ follows

$$B^2(\omega) = \begin{cases} A^2\exp\left[-\left(\dfrac{\omega-\omega_m}{\delta_\omega}\right)^2\right] & \text{for } \omega_{lc}\leqslant\omega\leqslant\omega_{uc}, \\ 0 & \text{otherwise}, \end{cases} \tag{6}$$

where the term A^2 can be written as (Glauert and Horne, 2005)

$$A^2 = \frac{2}{\sqrt{\pi}}\frac{|B_\omega|^2}{\delta_\omega}\left[\mathrm{erf}\left(\frac{\omega_m-\omega_{lc}}{\delta_\omega}\right)+\mathrm{erf}\left(\frac{\omega_{uc}-\omega_m}{\delta_\omega}\right)\right]^{-1}, \tag{7}$$

with the upper and lower cut-off frequency ω_{uc} and ω_{lc}, peak frequency ω_m, spectral bandwidth δ_ω, and averaged wave amplitude B_ω. The wave normal angle distribution is given by

$$g(X) = \exp\left[-\left(\frac{X-X_m}{X_\omega}\right)^2\right], \tag{8}$$

where X=tan(θ), X_m=tan(θ_m), X_ω=tan(δ_θ) with the wave normal angle θ, peak wave normal angle θ_m, and angular width δ_θ. The wave spectral intensity is further assumed constant within the wave latitudinal coverage.

For the sake of the sensitivity analysis of chorus wave scattering rates in the Jovian radiation belts, we select the following group of the above ambient and wave parameters as the representative standard for quantitative comparisons: L_J = 8; the dipole magnetic field model given by equation (1) with B_0=0.42 mT; the cold

plasma Density Model 1 (DM1) given by equation (2); the wave frequency spectrum: B_ω=20 pT, ω_m/Ω_e=0.1, δ_ω/Ω_e=0.05, ω_{lc}/Ω_e=0.05, and ω_{uc}/Ω_e=0.25, where Ω_e is the equatorial electron gyrofrequency; the wave normal angle distribution: θ_m =0°, δ_θ=30°, θ_{lc}=0°, and θ_{uc}=70°; and the wave latitudinal coverage λ_m = 15°. In the following section, we vary one input parameter reasonably but fix all the other input parameters to investigate the dependence of electron scattering rates on any specific parameter of interest.

3. Sensitivity Analysis Results of Chorus Wave Induced Electron Scattering Rates in the Jovian Magnetosphere

In this section, before we display the results of chorus wave induced electron scattering rates corresponding to various choices of ambient and wave parameters, we evaluate the variations of the wave dispersion curve and resonant wave frequency with a number of key input parameters. Figures 2a–2c present the quantitative results of chorus wave dispersion curve at the magnetic equator of L_J = 8 for varying magnitudes of the ambient magnetic field (B_0/2, B_0, and 2B_0), background plasma density (N_e/2, N_e, and 2N_e) and wave normal angle (θ = 0°, 15°, and 30°). Clearly, the chorus wave dispersion in the Jovian magnetosphere depends largely on all these parameters. Specifically, the increase trend of wave number (k) with wave frequency (ω) becomes more pronounced as the ambient magnetic field strength drops, the background plasma density increases or the wave normal angle increases. Figures 2d–2f show the variation of wave resonant frequency with magnetic latitude for the same varying parameter conditions above, corresponding to the first order (n = 1) cyclotron resonance with Jovian radiation belt electrons at 1 MeV and 10° equatorial pitch angle (α_0). Apparently, the resonant wave frequency increases with the magnetic latitude. In addition, the resonant wave frequency increases largely as the ambient magnetic field strength drops or the background plasma density increases, while it changes slightly with the wave normal angle. As a consequence, both the chorus wave dispersion relation and wave-particle resonant interaction condition need to be carefully determined for various sets of input parameters.

These input parameters under our consideration include the ambient magnetic field strength, background plasma density profile, peak wave normal angle, wave latitudinal coverage, peak wave frequency, wave spectral bandwidth, and Jovian L-shell. We do not consider the effect of chorus wave amplitude, since wave induced quasi-linear diffusion coefficients for different wave powers can be readily obtained by scaling the square of wave amplitude when the wave power is not strong enough to trigger nonlinear

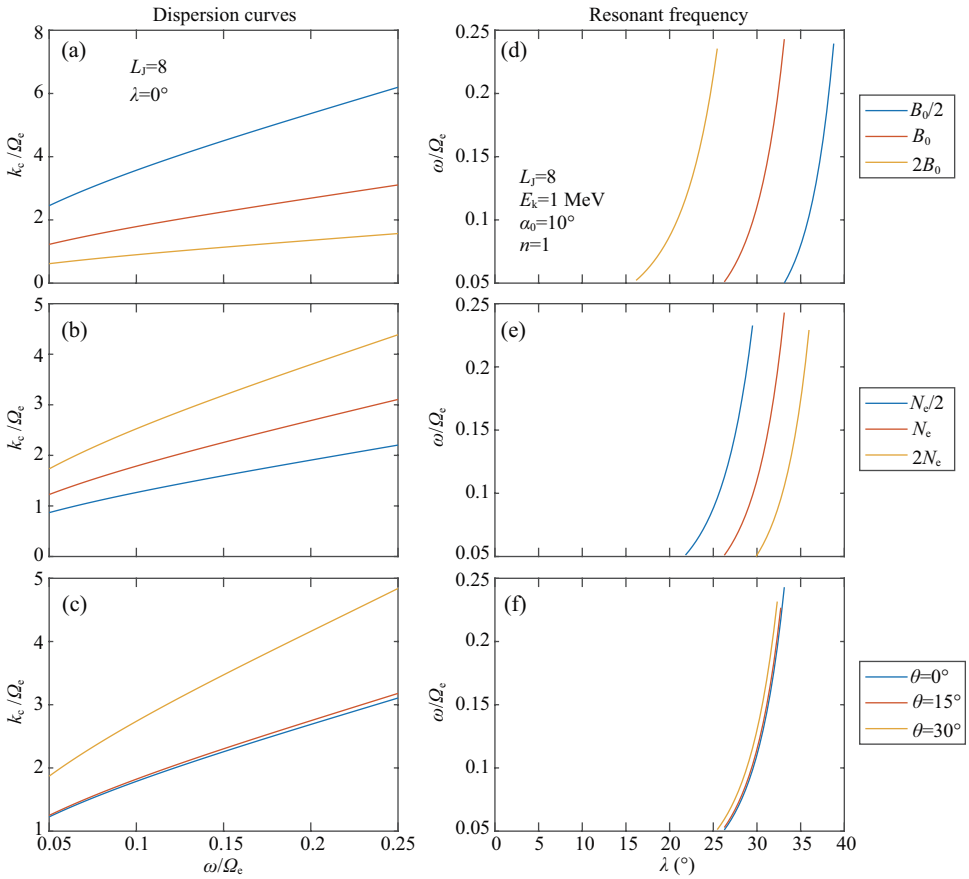

Figure 2. Chorus wave dispersion curves at the magnetic equator of L_J = 8 for varying magnitudes of (a) the ambient magnetic field (B_0/2, B_0, and 2B_0), (b) background plasma density (N_e/2, N_e, and 2N_e) and (c) wave normal angle (θ = 0°, 15°, and 30°). (d–f) Corresponding to (a–c), variation of wave resonant frequency with magnetic latitude for the first order (n = 1) cyclotron resonance with Jovian radiation belt electrons at 1 MeV and 10° equatorial pitch angle (α_0).

wave-particle interaction effects. The quasi-linear Full Diffusion Code (Ni et al., 2008, 2011, 2015) is implemented for various numerical runs to compute the chorus induced electron scattering rates in the Jovian magnetosphere, for which the contributions from the $n = -5$ to $n = 5$ cyclotron harmonic resonances and the Landau resonance ($n = 0$) are included.

3.1 Dependence on Ambient Magnetic Field Strength

To explore the dependence of chorus wave scattering rates on the ambient magnetic field amplitude, we follow the dipolar configuration (equation (1)) but scale the ambient magnetic field at $L_J = 8$. Specifically, three cases of $0.5B_0$, B_0, and $2B_0$ are adopted to approximately represent the conditions of stretched, normal and compressed ambient magnetic field, while all the other input parameters keep unchanged as shown in section 2. 2-D plots of bounce-averaged electron diffusion coefficients (i.e., pitch angle diffusion $<D_{\alpha\alpha}>$, momentum diffusion $<D_{pp}>$, and cross diffusion $<D_{\alpha p}>$) by chorus waves at $L_J = 8$ are presented in Figure 3 as a function of equatorial pitch angle (α_0) and electron kinetic energy (E_k).

Corresponding to the standard choice of input parameters, the middle panels (b, e, h) indicate that chorus waves can drive efficient pitch angle scattering on the order of 10^{-5} s^{-1} of ~100–150 keV electrons at pitch angles < ~55° and of ~150–500 keV electrons at pitch angles ~30°–70° in the Jovian radiation belts. The emissions can also cause more intense pitch angle scattering of ~100 keV–1 MeV electrons at pitch angles ~80°–85° at the rates approaching 10^{-4} s^{-1}, which is mainly due to the Landau resonance between the waves and the electrons. Hence, chorus waves can act as an important loss candidate of 100's keV electrons in the Jovian magnetosphere. In addition, these waves (with the assumed wave amplitude of 20 pT) can slowly accelerate ~100 keV–1 MeV electrons at the rates <~10^{-6} s^{-1} according to the momentum diffusion rates at high equatorial pitch angles > ~80°. It is worthwhile to note that the discontinuity of $<D_{pp}>$ at α_0 ~60° results from the wave confinement within 15° of the magnetic equator, which will be further studied in section 3.5.

When varying the ambient magnetic field strength of the Jovian magnetosphere, it is clearly shown that chorus wave scattering rate varies considerably. In general, compared to the results of the normal dipole field, the 2-D diffusion rate profile tends to shift downwards (upwards) as a whole when the ambient magnetic field decreases (increases). The maximal values of chorus wave scattering rates increase and tend to peak at electron energies well below 100 keV (not shown in Figure 3) when the ambient

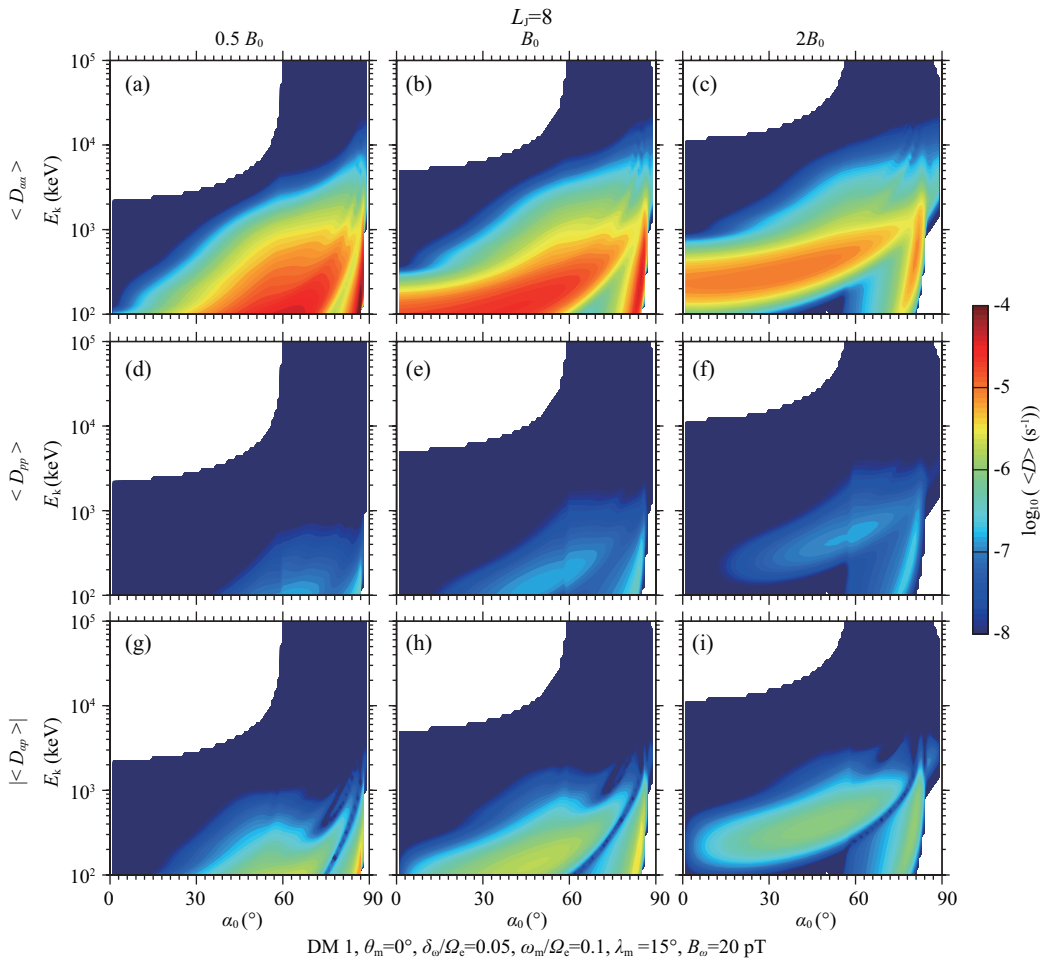

Figure 3. 2-D plot of chorus induced electron diffusion coefficients at $L_J = 8$ as a function of equatorial pitch angle α_0 and electron kinetic energy E_k: (a–c) pitch angle diffusion $<D_{\alpha\alpha}>$, (d–f) momentum diffusion $<D_{pp}>$, and (g–i) cross diffusion $<D_{\alpha p}>$, for three cases of (from left to right) $0.5B_0$, B_0, and $2B_0$ with B_0 as the normal dipole model intensity.

magnetic field decreases, while they decrease and peak at energies of ~200–300 keV when the ambient magnetic field increases. It is interesting to see that $<D_{pp}>$ strongly intensifies at energies > ~1 MeV for the case of $2B_0$, suggesting the enhanced acceleration effect of chorus waves on higher energy electrons.

The differences in chorus wave scattering rates induced by the variation of ambient magnetic field strength can be further evaluated by computing the normalized difference (ND) between any two models as follows:

$$\mathrm{ND} = 2.0\frac{<D>_2 - <D>_1}{<D>_2 + <D>_1} \times 100\%, \tag{9}$$

where $<D>_2$ denotes the chorus wave scattering rates using the varied model and $<D>_1$ denotes the results using the standard inputs given in section 2. Figure 4 presents the results of normalized difference for $<D_{\alpha\alpha}>$ and $<D_{pp}>$, compared to the results of the normal dipole field. Apparently, for the (E_k, α_0) space of our interest, the scattering rates primarily decrease but considerably increase at pitch angles ~50°–75° for 100's keV electrons and ~85° up to a few MeV electrons when the ambient magnetic field decreases. The variation trend is almost contrary when the ambient magnetic field increases, exhibiting large increase in diffusion rates over the majority of the space but large decrease in diffusion rates at pitch angles < ~70° for 100's keV electrons and ~80°–85° up to a few MeV electrons. Figures 3 and 4 clearly demonstrate that chorus wave induced electron scattering rates strongly depend on the profile of ambient magnetic field in the Jovian magnetosphere. Note that, while introducing large variations in chorus wave scattering rates, changes in B_0 can have a trivial effect when the bounce-averaged diffusion coefficients are negligibly small.

3.2 Dependence on Background Plasma Density Profile

To investigate the dependence of chorus wave scattering rates on background plasma density, we use the three density models given by equations (2)–(4) (defined as DM1–DM3) to compare the bounce-averaged electron diffusion coefficients, the results of which are shown in Figure 5. Basically, the chorus wave scattering rates do not exhibit large variations for the three considered plasma density models.

Figure 6 shows the results of normalized difference for $<D_{\alpha\alpha}>$ and $<D_{pp}>$, compared to the results of DM1. Here $<D>_1$ in equation (9) denotes the chorus wave scattering rates obtained using the constant plasma density model (DM1). It is clearly shown that the scattering rates are almost identical between DM1 and DM3. In contrast, the electron scattering rates for DM2 exhibit large increases for electrons at energies of 300 keV–5MeV with equatorial pitch angles <~20°. While the normalized differences are also large between DM1 and DM2 for >5 MeV electrons at equatorial pitch angles up to ~60°, the corresponding scattering rates are negligibly small. Figures 5 and 6 indicate that electron scattering rates by equatorial ($|\lambda| < 15°$) chorus waves in the Jovian magnetosphere vary insignificantly with the three ambient plasma density models that are adopted on basis of previous empirical studies.

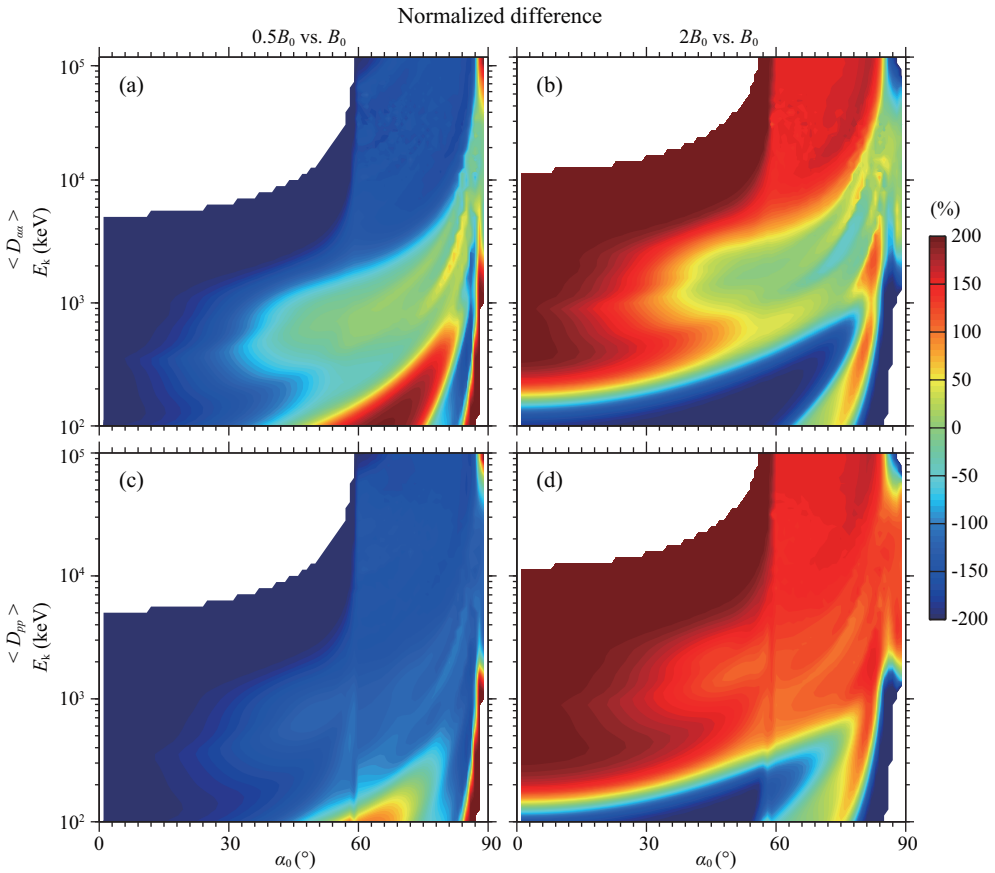

Figure 4. Corresponding to Figure 3, 2-D plots of normalized difference for (top panels) $<D_{\alpha\alpha}>$ and (bottom panels) $<D_{pp}>$.

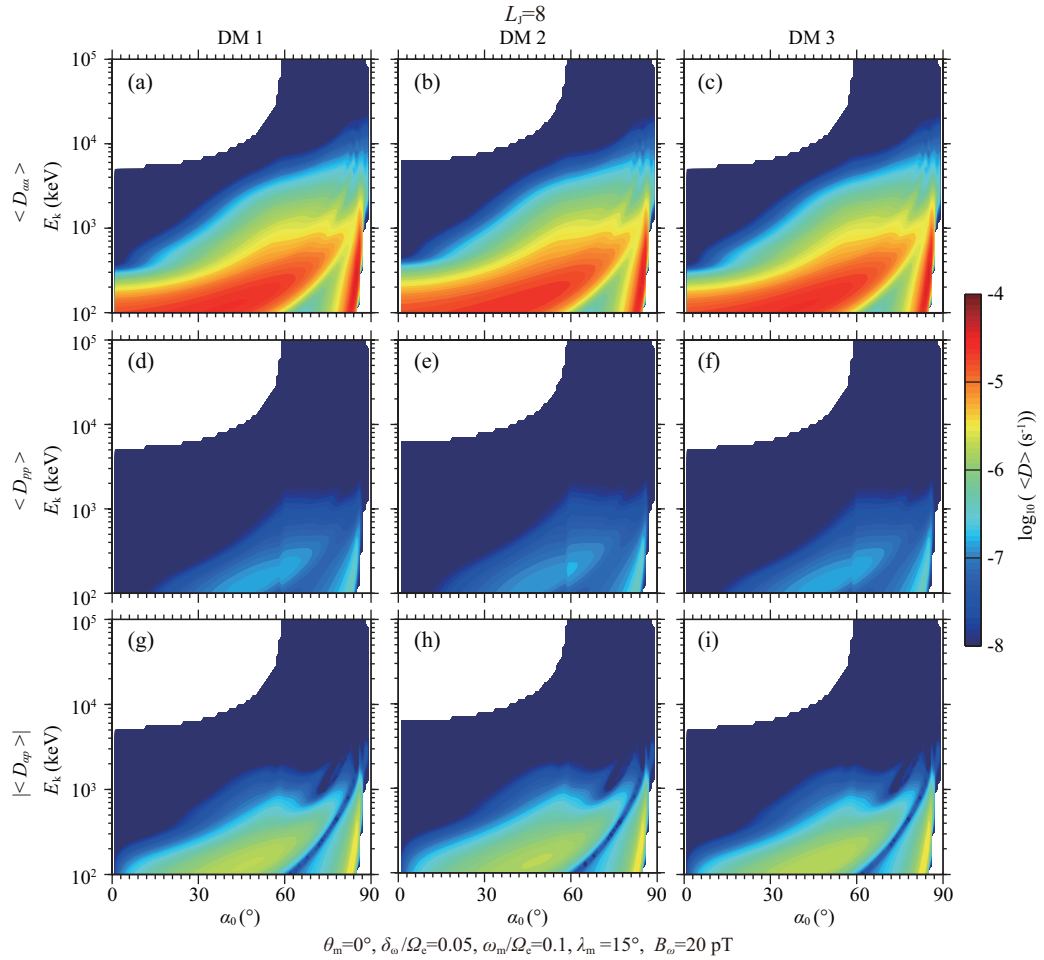

Figure 5. Same as in Figure 3, except for three different background plasma density profiles given by equations (1)–(3), i.e., DM1, DM2 and DM3.

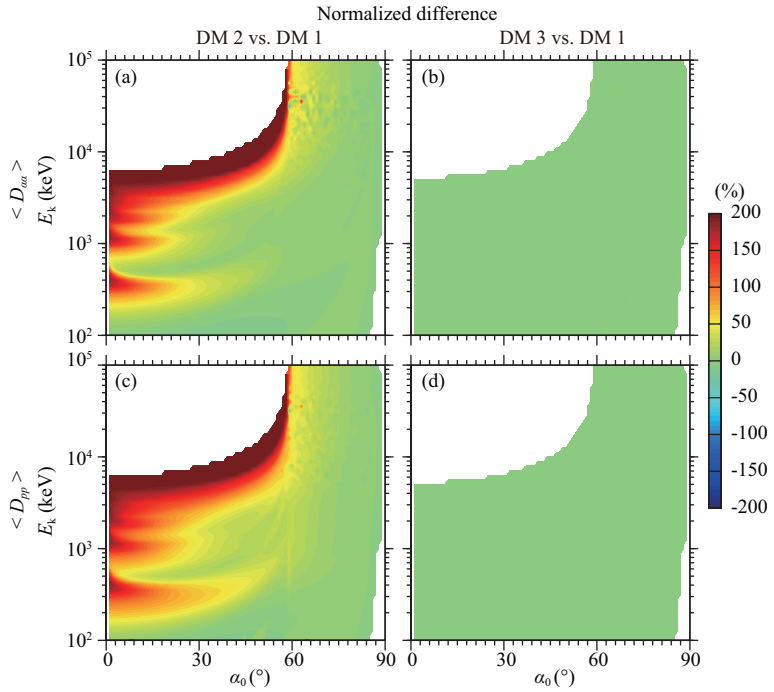

Figure 6. Corresponding to Figure 5, 2-D plots of normalized difference for (top panels) <$D_{\alpha\alpha}$> and (bottom panels) <D_{pp}>.

3.3 Dependence on Peak Wave Normal Angle

To study the dependence of chorus wave scattering rates on peak wave normal angle θ_m, we choose three cases as follows: θ_m =0°, θ_m =30° and the latitudinally varying model (e.g., Tao et al., 2011): θ_m=−0.36+5.04λ−0.06λ^2. Figure 7 shows the 2-D plots of bounce-averaged electron diffusion coefficients corresponding to the three peak wave normal angle models.

Clearly, chorus wave scattering rates in the Jovian magnetosphere vary with the adopted peak wave normal angle. Specifically, larger peak wave normal angle tends to decrease the scattering rates for 100's keV electrons at a broad range of equatorial pitch angles up to ~80° but increase the scattering rates for higher energy electrons at small and intermediate pitch angles. Such a tendency becomes more distinct by computing the normalized differences of the diffusion coefficients between different peak wave normal angle models, the results of which are presented in Figure 8.

Here $<D>_1$ in equation (9) denotes the chorus wave scattering rates obtained with θ_m =0°. It is clear that, as a result of increasing peak wave normal angle, the scattering rates increase significantly for ~ 300 keV–5 MeV electrons with equatorial pitch angles <~45°. In contrast, the scattering rates decrease more or less at energies of ~5–100 MeV with equatorial pitch angles ~60°–75°, while the value of scattering rates in these corresponding regions are small. Figures 7 and 8 together illustrate that chorus wave induced electron scattering rates depend on peak wave normal angle in the Jovian magnetosphere.

3.4 Dependence on Wave Latitudinal Coverage

As shown in Figures 3, 5, and 7, there exists a discontinuity in the energy diffusion coefficients $<D_{pp}>$ at the equatorial pitch angle ~59°. In order to explain this phenomenon, here we choose three wave latitudinal coverage, say, $|\lambda|$ < 15°, $|\lambda|$ < 30° and $|\lambda|$ < 40° to compute the bounce-averaged diffusion coefficients, the results of which are displayed in Figure 9.

It is clear that the pitch angle scattering coefficients increase substantially for ~200keV–1MeV electrons at equatorial pitch angles < ~40° when the wave latitudinal coverage increases to 30°. The region of diffusion rate increase expands to higher energies and larger equatorial pitch angles when chorus waves occur at $|\lambda|$ < 40°. Regarding the momentum diffusion coefficients, the increase is obvious for ~100–1 MeV electrons at pitch angles ~20°–60° between the cases of $|\lambda|$ < 15° and $|\lambda|$ < 30°, while the variation is small between the cases of $|\lambda|$ < 30° and $|\lambda|$ < 40°. Also interest-

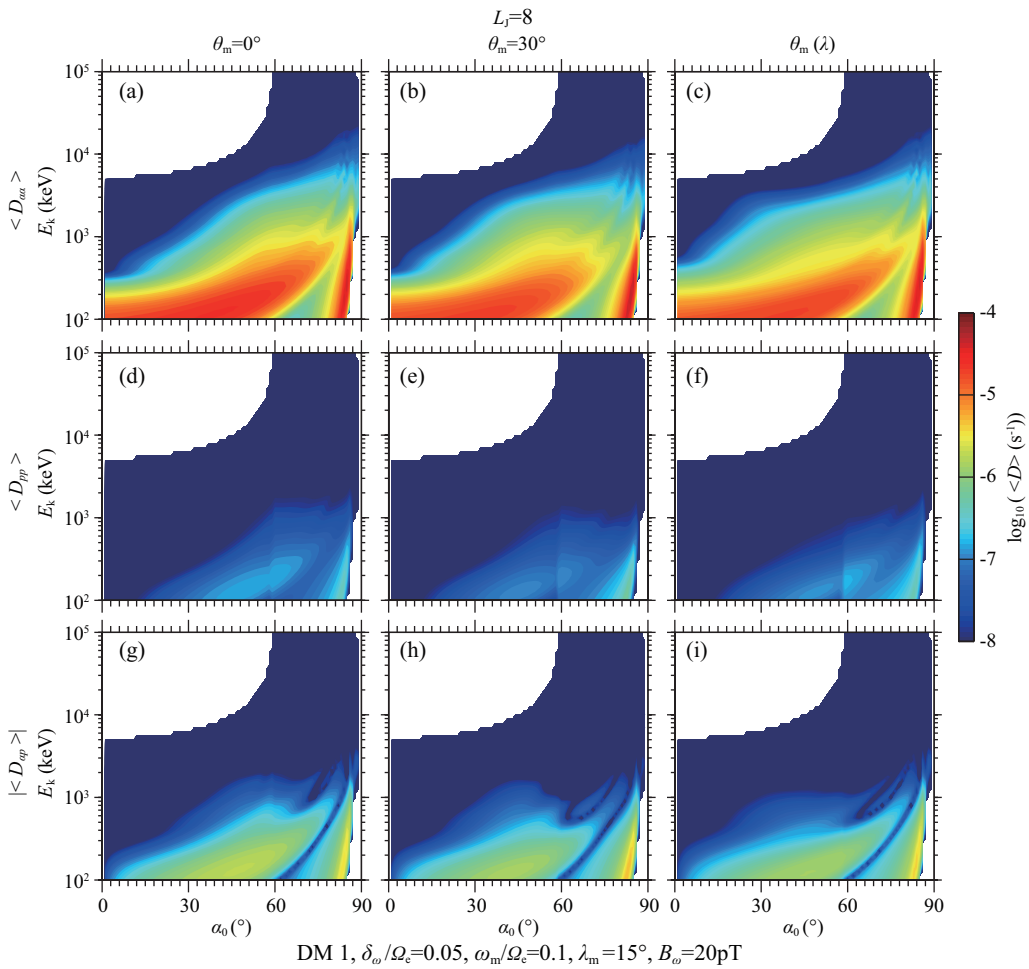

Figure 7. Same as in Figure 3, except for three different values of peak wave normal angle, i.e., θ_m = 0°, θ_m =30° and the latitudinally varying model θ_m=−0.36+5.04λ−0.06λ^2.

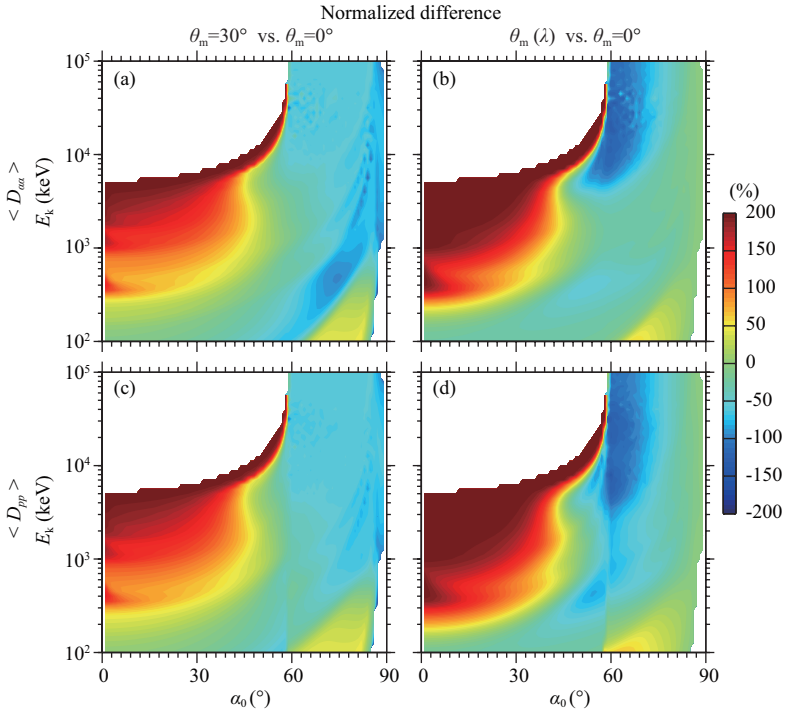

Figure 8. Corresponding to Figure 7, 2-D plots of normalized difference for (top panels) $<D_{\alpha\alpha}>$ and (bottom panels) $<D_{pp}>$.

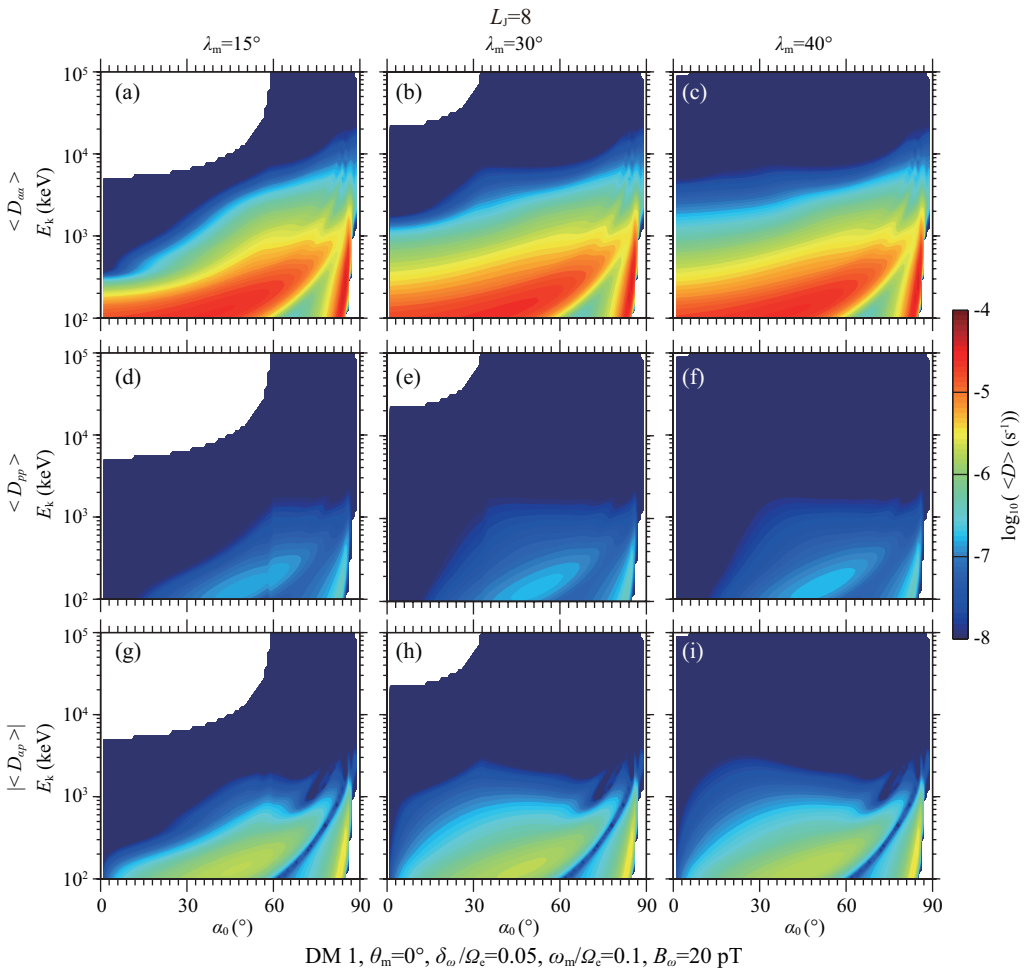

Figure 9. Same as in Figure 3, except for three different cases of wave latitudinal coverage, i.e., $|\lambda| < 15°$, $|\lambda| < 30°$ and $|\lambda| < 40°$.

ingly, the discontinuity in $<D_{pp}>$ at pitch angle ~59° when $|\lambda| < 15°$ disappears when chorus waves have a larger latitudinal coverage, as shown in the second and third columns of Figure 9, demonstrating that the wave latitudinal extent acts as an important factor contributing to electron scattering rates in the Jovian radiation belts.

Figure 10 shows the results of normalized difference for $<D_{\alpha\alpha}>$ and $<D_{pp}>$, compared to the results for the case of $|\lambda| < 15°$. Here $<D>_1$ in equation (9) denotes the chorus wave scattering rates obtained with $|\lambda| < 15°$. It is clear that the normalized differences are large for ~200 keV–100 MeV electrons at equatorial pitch angles up to ~60°. In contrast, the scattering rates at higher pitch angles do not show any change because these electrons can only bounce to the mirror latitude ~15° and thus chorus waves at $|\lambda| > 15°$ have no effect on them. Figures 9 and 10 clearly indicate that the wave latitudinal coverage in the Jovian magnetosphere strongly affects chorus wave scattering rates of electrons that mirror above the wave latitudinal extent.

3.5 Dependence on Peak Wave Frequency

To investigate the dependence of chorus wave scattering rates on peak wave frequency ω_m, we choose three typical values of ω_m/Ω_e, i.e., 0.1, 0.15, and 0.2, to compare the computed bounce-averaged diffusion coefficients, the results of which are shown in Figure 11.

When varying the peak wave frequency of whistler-mode chorus in the Jovian magnetosphere, chorus induced electron scattering rates vary considerably. As the peak wave frequency increases, the pitch angle diffusion coefficients overall shift downwards, thereby causing the rates to decrease at a broad range of considered energy and pitch angle but increase at a small region, e.g., ~100 keV with equatorial pitch angles ~50°–70°. The variation of momentum diffusion coefficients is also clear to illustrate that their maximal values increase considerably and tend to peak at electron energies below 100 keV (not shown in Figure 11).

Figure 12 shows the results of normalized difference for $<D_{\alpha\alpha}>$ and $<D_{pp}>$, compared to the results for the case of $\omega_m/\Omega_e = 0.1$. Here $<D>_1$ in equation (9) denotes the chorus wave scattering rates obtained with $\omega_m/\Omega_e = 0.1$. More clearly, when the value of ω_m/Ω_e increases, $<D_{\alpha\alpha}>$ increases for ~100 keV–1 MeV with equatorial pitch angles ~45°–80° but predominantly decreases at the other regions. A similar variation trend occurs for $<D_{pp}>$, while the degree of either increase or decrease of scattering rates tends to be smaller. It is also interesting to see that $<D_{pp}>$ is more likely to increase for electrons with equatorial pitch angles ~45°–80°. Figures 11 and 12 clearly demonstrate that chorus wave induced electron scattering rates strongly depend on the peak wave frequency in the Jovian magnetosphere.

3.6 Dependence on Wave Spectral Bandwidth

To study the dependence of chorus wave scattering rates on chorus wave spectral bandwidth, we choose three values of δ_ω/Ω_e, i.e., 0.05, 0.1, and 0.15, to compute the bounce-averaged electron dif-

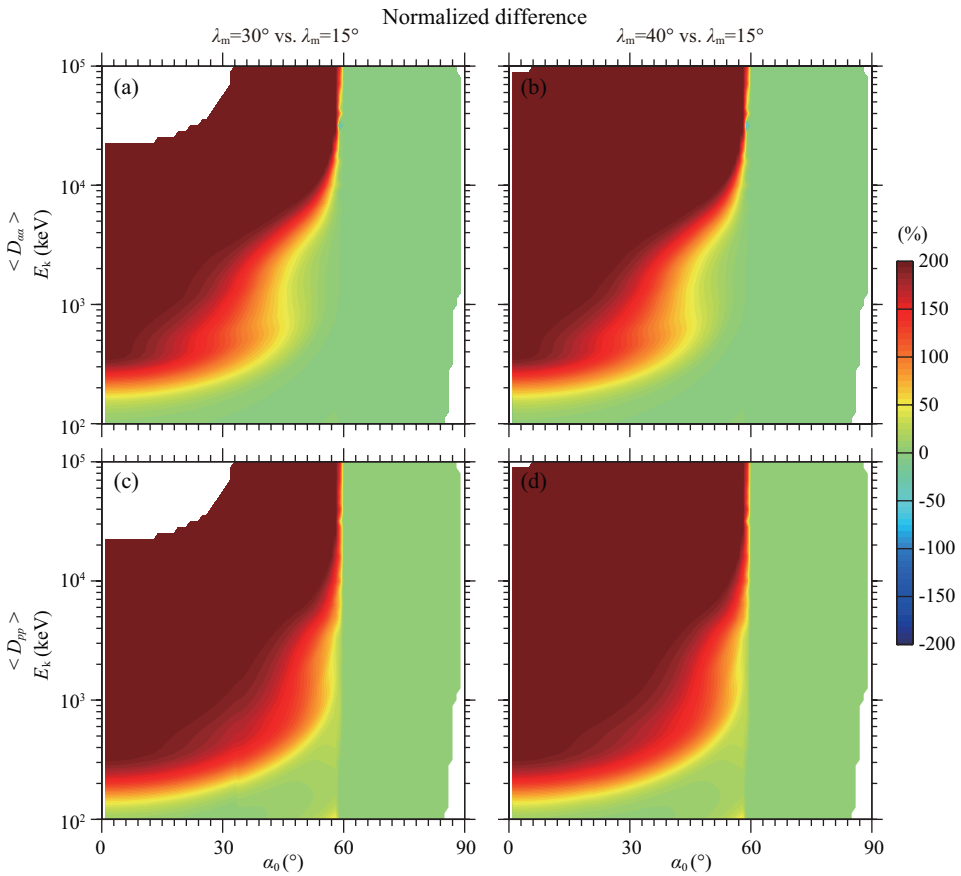

Figure 10. Corresponding to Figure 9, 2-D plots of normalized difference for (top panels) $<D_{\alpha\alpha}>$ and (bottom panels) $<D_{pp}>$.

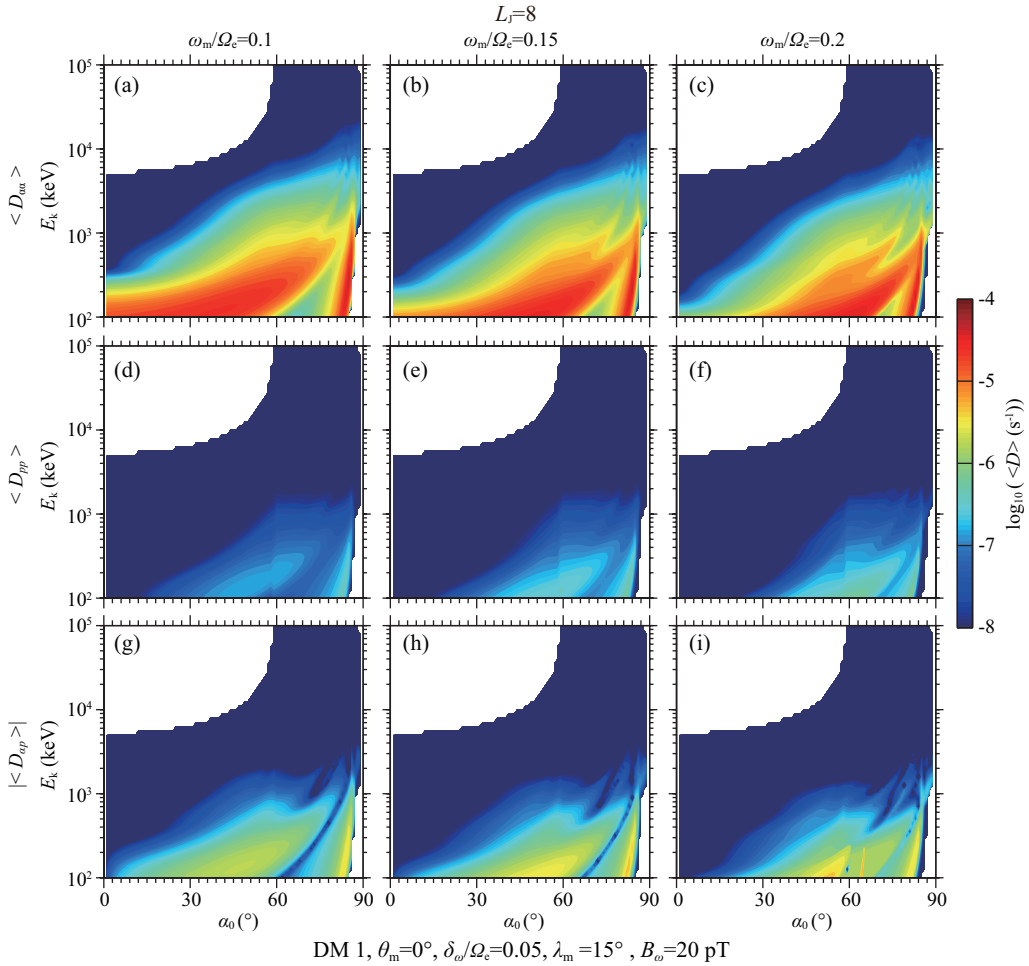

Figure 11. Same as in Figure 3, except for three different cases of peak wave frequency, i.e., ω_m/Ω_e = 0.1, 0.15 and 0.2.

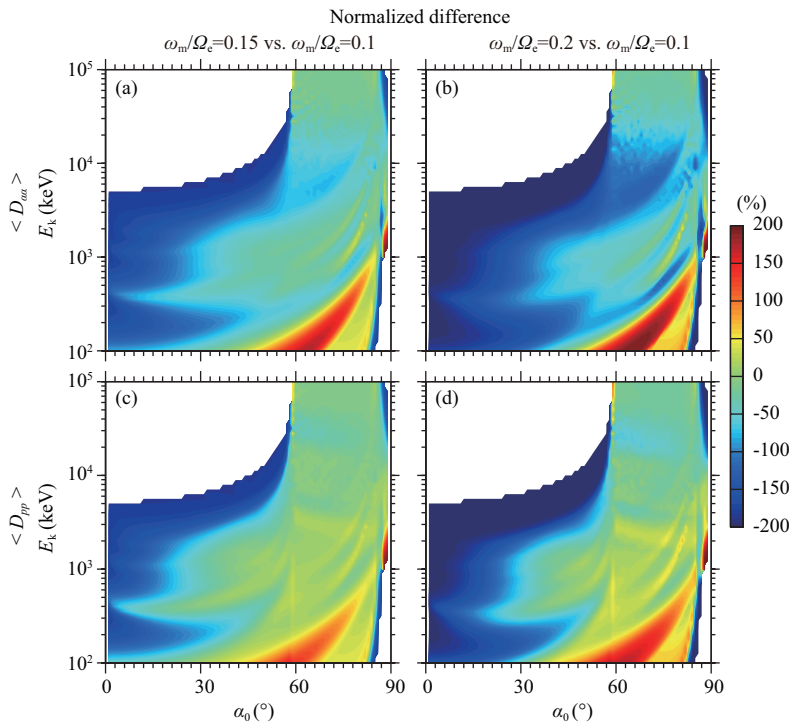

Figure 12. Corresponding to Figure 11, 2-D plots of normalized difference for (top panels) <$D_{\alpha\alpha}$> and (bottom panels) <D_{pp}>.

fusion coefficients at L_J = 8 in the Jovian magnetosphere, the results of which are displayed in Figure 13 for comparisons.

As the wave spectral bandwidth increases, chorus induced electron scattering rates vary discernibly but slightly. Specifically, the peak values of $<D_{\alpha\alpha}>$ somehow decrease and the strong scattering rates >10^{-5} s^{-1} extend to a broader region with increasing values of δ_ω/Ω_e. In contrast, the maximal values of $<D_{pp}>$ increase and tend to peak at electron energies <100 keV (not shown in Figure 13) when the chorus wave spectral bandwidth increases.

Figure 14 displays the results of normalized difference for $<D_{\alpha\alpha}>$ and $<D_{pp}>$, compared to the results of δ_ω/Ω_e=0.05. Here $<D>_1$ in equation (9) denotes the chorus wave scattering rates obtained with δ_ω/Ω_e=0.05. Clearly, the chorus wave scattering coefficients vary largely only for a narrow range of electron energy and equatorial pitch angle, say, for ~100 keV–1 MeV electrons with a small portion of equatorial pitch angles between ~50° and 80° and for 1–2 MeV with equatorial pitch angles ~85°. Figures 13 and 14 indicate that chorus wave induced electron scattering rates weakly depend on the wave spectral bandwidth in the Jovian magnetosphere.

3.7 Dependence on Jovian *L*-shell

To explore the dependence of chorus wave scattering rates on Jovian *L*-shell (L_J), we select three L_J values, that is, L_J = 6, 8, and 10, to compute and compare chorus induced bounce-averaged diffusion coefficients at different regions of the Jovian radiation belts. Figure 15 shows the 2-D plots of bounce-averaged electron diffusion coefficients by chorus waves as a function of equatorial pitch angle and electron kinetic energy at the three indicated Jovian *L*-shells.

It is evident that given chorus wave amplitude, electron scattering rates increase considerably as the Jovian *L*-shell increases. In order to carefully check the underlying relationship between electron diffusion coefficients by chorus and Jovian *L*-shell, we assume that electron scattering rates are proportional to L_J^3 and then evaluate the ratios between the diffusion coefficients at two Jovian *L*-shells, i.e.,

$$\mathrm{RR} = \left(<D>_1/{L_{J1}}^3\right)/\left(<D>_2/{L_{J2}}^3\right), \tag{10}$$

where $<D>_1$ denotes the chorus wave scattering rates at L_{J1} and $<D>_2$ denotes the chorus wave scattering rates at L_{J2}. Figure 16 displays the results of the ratio RR for two groups of comparison, say, L_J = 6 versus L_J = 8 and L_J = 10 versus L_J = 8. It is clearly illustrated that in the majority of the (E_k, α_0)-space considered in this study, the ratio is close to 1, strongly suggesting that an approximately good power law function seems to exist between chorus

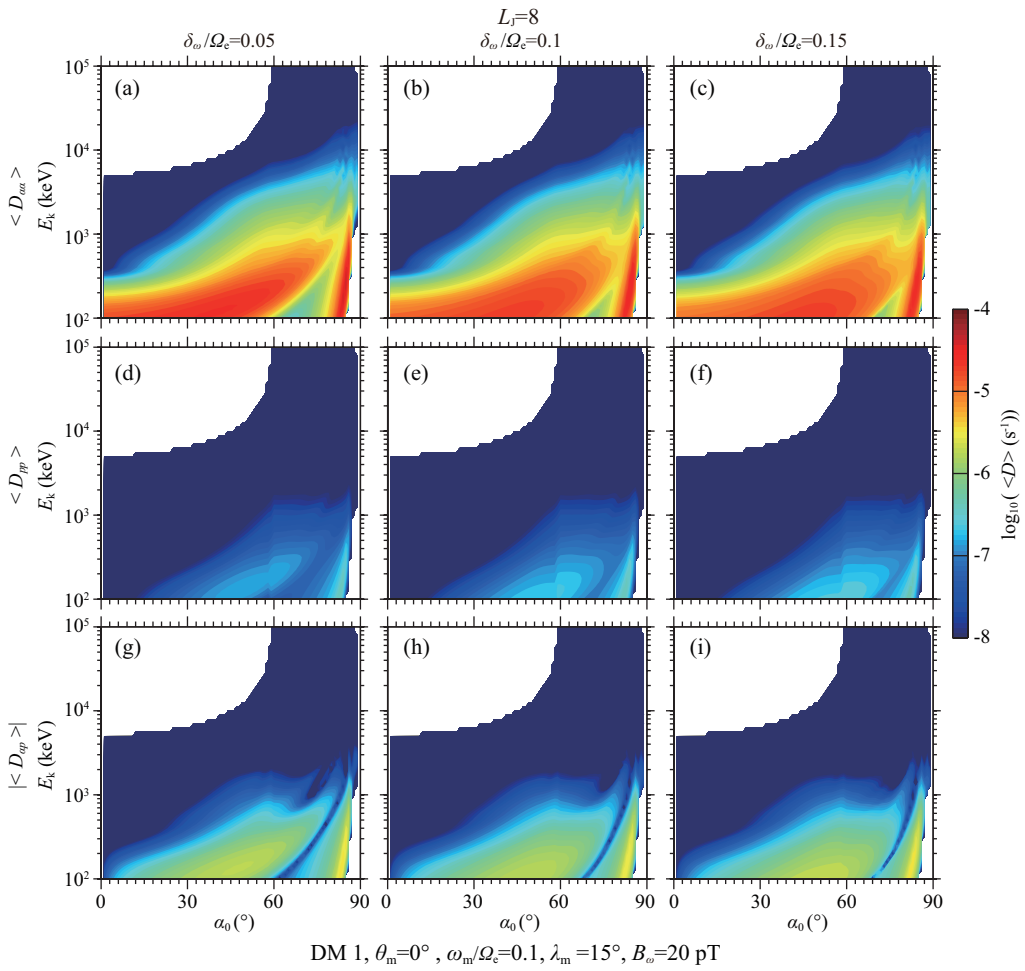

Figure 13. Same as in Figure 3, except for three different cases of wave spectral bandwidth, i.e., ω_m/Ω_e = 0.1, 0.15 and 0.2.

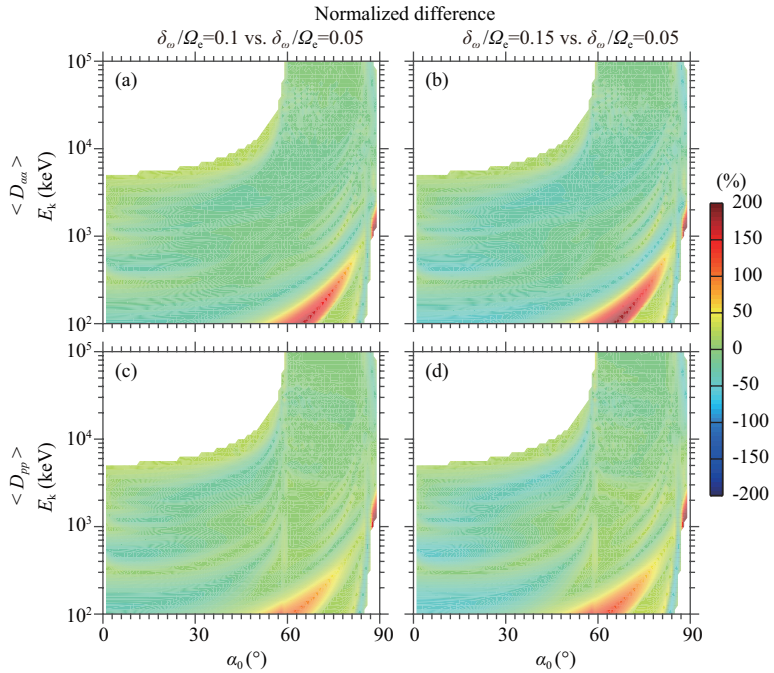

Figure 14. Corresponding to Figure 13, 2-D plots of normalized difference for (top panels) $<D_{\alpha\alpha}>$ and (bottom panels) $<D_{pp}>$.

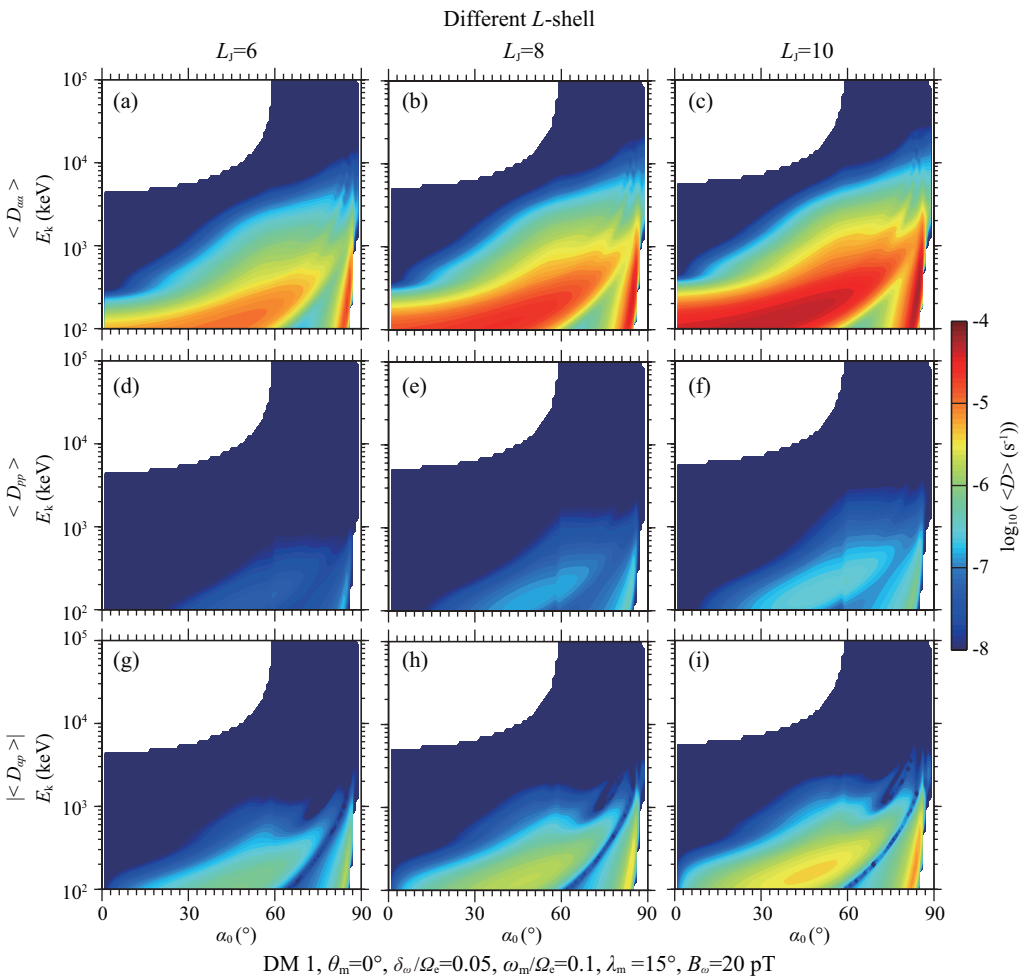

Figure 15. 2-D plot of chorus induced electron diffusion coefficients as a function of equatorial pitch angle α_0 and electron kinetic energy E_k for three Jovian L-shells (from left to right): L_J = 6, 8 and 10.

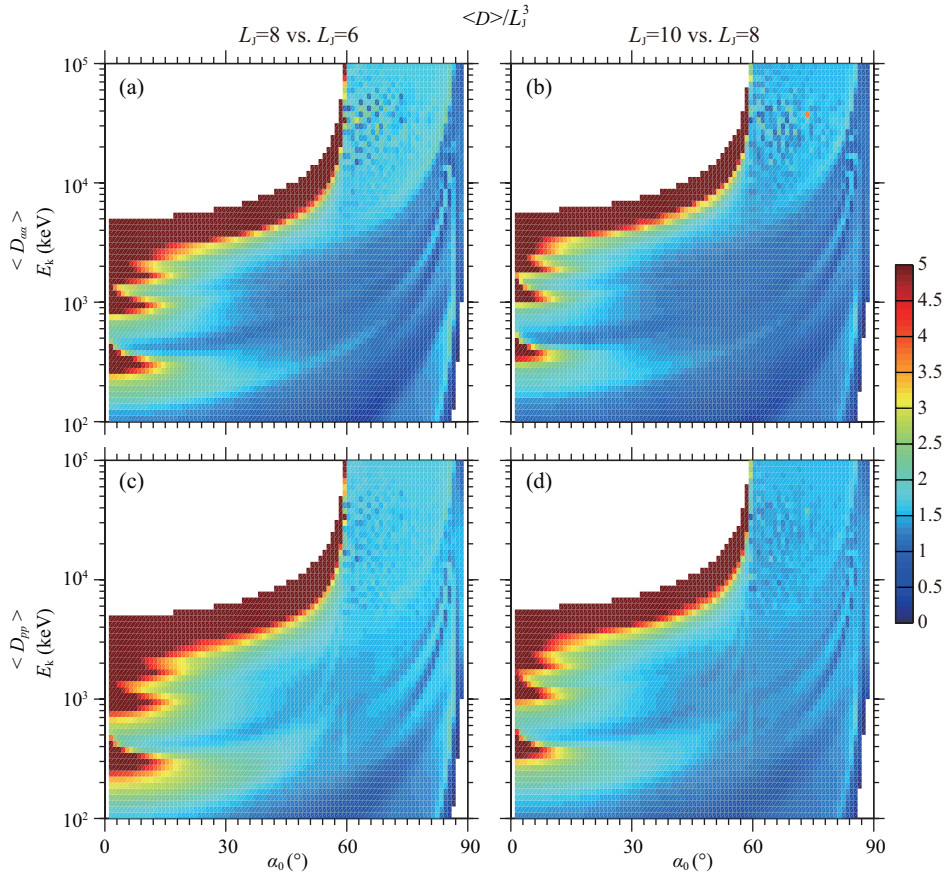

Figure 16. Corresponding to Figure 15, (a) ($<D_{\alpha\alpha}>|_{L_J=8}/8^3$)/($<D_{\alpha\alpha}>|_{L_J=6}/6^3$), (b) ($<D_{\alpha\alpha}>|_{L_J=10}/10^3$)/($<D_{\alpha\alpha}>|_{L_J=8}/8^3$), (c) ($<D_{pp}>|_{L_J=8}/8^3$)/($<D_{pp}>|_{L_J=6}/6^3$), and (d) ($<D_{pp}>|_{L_J=10}/10^3$)/($<D_{pp}>|_{L_J=8}/8^3$), which indicates that chorus induced electron scattering rates exhibit a tendency to be approximately proportional to L_J^3.

induced electron scattering rates and Jovian *L*-shell, that is, $<D>$ is approximately proportional to L_J^3, given the chorus wave amplitude. There are exceptions at small equatorial pitch angles or high electron energies (indicated by the red areas in Figure 16), which however mostly correspond to very small rates of chorus wave scattering. Figures 15 and 16 clearly clarify that chorus wave induced electron scattering rates strongly depend on *L*-shell in the Jovian magnetosphere.

4. Discussions and Conclusions

Populated by energetic and relativistic electrons at energies from ~100 keV to 100 MeV, the Jovian radiation belts are regarded as the most intense particle radiation environment in the solar planets. While its formation remains unresolved, a number of mechanisms have been proposed as candidate contributors, including local acceleration due to electron cyclotron resonance with whistler-mode chorus. In the quasi-linear regime, computation of electron scattering rates by chorus waves provides straightforward messages of the wave impact on electron dynamics in the Jovian radiation belts, which however requires detailed information of both ambient magnetic field and plasma density and wave spectral property. Hence, to comprehend the resonant wave-particle interactions in the Jovian magnetosphere, we have implemented a detailed analysis to investigate how quasi-linear bounce-averaged electron diffusion coefficients induced by whistler-mode chorus depend on a full group of important ambient magnetospheric and wave parameters.

Our main conclusions are summarized as follows:

(1) Factors that can strongly affect chorus induced quasi-linear electron scattering rates include the ambient magnetic field intensity, the wave latitudinal coverage, and the peak frequency and bandwidth of the wave spectral distribution in the Jovian magnetosphere.

(2) Chorus induced quasi-linear electron scattering rates in the Jovian radiation belts tend to depend slightly on the background plasma density profile and the peak wave normal angle, especially when the wave emissions are confined at low latitudes (e.g., $|\lambda| < 15°$).

(3) Given the chorus wave amplitude, chorus induced electron scattering rates strongly depend on Jovian *L*-shell to exhibit a tendency approximately proportional to L_J^3.

Our comprehensive analysis explicitly demonstrates the importance of reliable information of both the ambient magnetospheric state and wave distribution property to understanding the contribution of whistler-mode chorus to the dynamic electron evolution in the Jovian radiation belts and therefore has implications for future mission planning to explore the extreme particle radiation environment of Jupiter and its satellites.

Acknowledgements

This work was supported by the NSFC grants (41674163) and (41474141), by Lunar and Planetary Science Laboratory, Macau University of Science and Technology—Partner Laboratory of Key Laboratory of Lunar and Deep Space Exploration, Chinese Academy of Sciences (FDCT No. 039/2013/A2), and by the Hubei Province Natural Science Excellent Youth Foundation (2016CFA044).

References

Bagenal, F., and Delamere, P. A. (2011). Flow of mass and energy in the magnetospheres of Jupiter and Saturn. *J. Geophys. Res.*, *116*, A05209. https://doi.org/10.1029/2010JA016294

Berge, G. L., and Gulkis, S. (1976). Earth-based observations of Jupiter: Millimeter to meter wavelengths. Tech. Rep., Univ. of Arizona Press, Tucson, Arizona.

Bolton, S. J., Janssen, M., Thorne, R., Levin, S., Klein, M., Gulkis, S., Bastian, T., Sault, R., Elachi, C., Hofstadter, M., Bunker, A., Dulk, G., Gudim, E., Hamilton, G., Johnson, W. T. K., Leblanc, Y., Liepack, O., McLeod, R., Roller, J., Roth, L., and West, R. (2002). Ultra-relativistic electrons in Jupiter's radiation belts. *Nature*, *415*(6875), 987–991. https://doi.org/10.1038/415987a

Burke, B. F., and Franklin, K. L. (1955). Observations of a variable radio source associated with the planet Jupiter. *J. Geophys. Res.*, *60*(2), 213–217. https://doi.org/10.1029/JZ060i002p00213

Carr, T. D., and Gulkis, S. (1969). The magnetosphere of Jupiter. *Annu. Rev. Astron. Astrophys.*, *7*, 577–618. https://doi.org/10.1146/annurev.aa.07.090169.003045

de Soria-Santacruz, M., Garrett, H. B., Evans, R. W., Jun, I., Kim, W., Paranicas, C., and Drozdov, A. (2016). An empirical model of the high-energy electron environment at Jupiter. *J. Geophys. Res. Space Physics*, *121*, 9732–9743. https://doi.org/10.1002/2016JA023059

Drake, F. D., and Hvatum, S. (1959). Non-thermal microwave radiation from Jupiter. *Astron. J.*, *64*, 329–330.

Gerard, E. (1970). Observations of Jupiter at 11.13 cm. *Astron. Astrophys.*, *8*, 181.

Gerard, E. (1976). Variation of the radio emission of Jupiter at 21.3 and 6.2 cm wavelength. *Astron. Astrophys.*, *50*, 353–360.

Glauert, S. A., and Horne, R. B. (2005). Calculation of pitch angle and energy diffusion coefficients with the PADIE code. *J. Geophys. Res.*, *110*, A04206. https://doi.org/10.1029/2004JA010851

Horne, R. B., Thorne, R. M., Glauert, S. A., Menietti, J. D., Shprits, Y. Y., and Gurnett, D. A. (2008). Gyro-resonant electron acceleration at Jupiter. *Nature Phys.*, *4*(4), 301–304. https://doi.org/10.1038/nphys897

Khurana, K. K. (1997). Euler potential models of Jupiter's magnetospheric field. *J. Geophys. Res.*, *102*(6), 11295–11306. https://doi.org/10.1029/97JA00563

Klein, M. J. (1976). The variability of the total flux density and polarization of Jupiter's decimetric radio emission. *J. Geophys. Res.*, *81*(19), 3380–3382. https://doi.org/10.1029/JA081i019p03380

Klein, M. J., Thompson, T. J., and Bolton, S. (1989). Systematic observations and correlation studies of variations in the synchrotron radio emission from Jupiter. In *Time Variable Phenomena in The Jovian System*. NASA Special Publication, vol. 494, pp.151–155.

Ni, B. B., Thorne, R. M., Shprits, Y. Y., and Bortnik, J. (2008). Resonant scattering of plasma sheet electrons by whistler-mode chorus: Contribution to diffuse auroral precipitation. *Geophys. Res. Lett.*, *35*, L11106. https://doi.org/10.1029/2008GL034032

Ni, B. B., Thorne, R. M., Meredith, N. P., Horne, R. B., and Shprits, Y. Y. (2011). Resonant scattering of plasma sheet electrons leading to diffuse auroral precipitation: 2. Evaluation for whistler mode chorus waves. *J. Geophys. Res.*, *116*, A04219. https://doi.org/10.1029/2010JA016233

Ni, B. B., Cao, X., Zou, Z. Y., Zhou, C., Gu, X. D., Bortnik, J., Zhang, J. C., Fu, S., Zhao, Z. Y., Shi, R., and Xie, L. (2015). Resonant scattering of outer zone relativistic electrons by multiband EMIC waves and resultant electron loss time scales. *J. Geophys. Res. Space Physics*, *120*, 7357–7373. https://doi.org/10.1002/2015JA021466

Persoon, A. M., Gurnett, D. A., Kurth, W. S., and Groene, J. B. (2006). A simple scale height model of the electron density in Saturn's plasmadisk. *Geophys. Res. Lett.*, *33*, L18106. https://doi.org/10.1029/2006GL027090

Radhakrishnan, V., and Roberts, J. A. (1960). Polarization and angular extent of the 960-Mc/sec radiation from Jupiter. *Phys. Rev. Lett.*, *4*(10), 493. https://doi.org/10.1103/PhysRevLett.4.493

Santos-Costa, D., and Bourdarie, S. A. (2001). Modeling the inner Jovian electron radiation belt including non-equatorial particles. *Planet. Space Sci.*, *49*, 303–312. https://doi.org/10.1016/S0032-0633(00)00151-3

Santos-Costa, D., Bolton, S. J., Thorne, R. M., Miyoshi, Y., and Levin, S. M. (2008). Investigating the origins of the Jovian decimetric emission's variability. *J. Geophys. Res.*, *113*, A01204. https://doi.org/10.1029/2007JA012396

Shprits, Y. Y., Menietti, J. D., Gu, X., Kim, K. C., and Horne, R. B. (2012). Gyroresonant interactions between the radiation belt electrons and whistler mode chorus waves in the radiation environments of Earth, Jupiter, and Saturn: A comparative study. *J. Geophys. Res.*, *117*(A11). https://doi.org/10.1029/2012JA018031

Tao, X., Thorne, R. M., Horne, R. B., Ni, B., Menietti, J. D., Shprits, Y. Y., and Gurnett, D. A. (2011). Importance of plasma injection events for energization of relativistic electrons in the Jovian magnetosphere. *J. Geophys. Res.*, *116*(A01). https://doi.org/10.1029/2010JA01610

Woodfield, E. E., Horne, R. B., Glauert, S. A., Menietti, J. D., and Shprits, Y. Y. (2013). Electron acceleration at Jupiter: Input from cyclotron-resonant interaction with whistler-mode chorus waves. In *Ann. Geophys.*, vol. 31, pp. 1619–1630, Copernicus GmbH.

Woodfield, E. E., Horne, R. B., Glauert, S. A., Menietti, J. D., and Shprits, Y. Y. (2014). The origin of Jupiter's outer radiation belt. *J. Geophys. Res.*, *119*(5), 3490–3502. https://doi.org/10.1002/2014JA019891